Supplement of Nat. Hazards Earth Syst. Sci., 24, 465–480, 2024
https://doi.org/10.5194/nhess-24-465-2024-supplement

Natural Hazards and Earth System Sciences
Open Access

Supplement of

Numerical-model-derived intensity–duration thresholds for early warning of rainfall-induced debris flows in a Himalayan catchment

Sudhanshu Dixit et al.

Correspondence to: Srikrishnan Siva Subramanian (srikrishnan@dm.iitr.ac.in)

Governing equations of the spatiotemporal debris flow numerical model:

To determine the rate of percolation water, the values of initial moisture content and hydraulic conductivity of the three soil layers are needed (the soil zone can be considered as a single layer too). For the calculation of the unsaturated hydraulic conductivity, the empirical soil-water characteristic curve (SWCC) by Farrell and Larson (1972) has been used, and the matric suction *|h|* (kPa) is defined as:

$$|h_1| = h_{A1} exp[\alpha_1(1 - S_1)];\ |h_2| = h_{A2} exp[\alpha_2(1 - S_2)]; |h_3| = h_{A3} exp[\alpha_3(1 - S_3)] \quad \text{S1}$$

where $|h_1|$, $|h_2|$, and $|h_3|$ (m) are the absolute values of matric suction head for soil layers 1, 2 and 3, h_{A1}, h_{A2}, and h_{A3} (m) are the absolute matric suctions at the air entry value, and α_1, α_2, and α_3 (dimensionless) are the slopes of the log-linear relationship of $ln(|h_1|)$ and (1-S_1). This relationship becomes valid whenever the matric suction increases above the air entry value.

Based on the SWCC of Farrell and Larson (1972), the relative hydraulic conductivity in unsaturated condition becomes:

$$k_r(\theta_1) = \theta_1{}^{\tau} \frac{[\exp(2\alpha 1\theta_{E1}) - 2\alpha 1\theta_{E1} - 1]}{[\exp(2\alpha 1) - 2\alpha 1 - 1]} \quad \text{S2}$$

where the tortuosity τ is assumed equal to 4/3 following Farrell and Larson (1972). The $k_r(\vartheta_E)$ is dimensionless, ranging from zero at the residual moisture content and one at complete saturation. The absolute unsaturated hydraulic conductivity, $k(\vartheta_1)$, is subsequently obtained by multiplying the relative hydraulic conductivity at unsaturated state with the saturated hydraulic conductivity k_{sat} (m/s). The same procedure is followed for the other two soil layers.

The lateral fluxes from the center of each pixel are modelled according to the following relationship (Beguería et al., 2009; Quenta et al., 2007):

$$Q = \frac{k_{sat} \times (Sin(W_f) \times CL \times t}{100} \quad \text{S3}$$

where Q is the lateral flux, W_f is the depth of wetting front, CL is the cell length (the resolution of the DEM), and t is the numerical timestep.

Once the volume of water outflowing from each pixel is known, it is routed both in the x and y directions according to the following formulae (Beguería et al., 2009):

$$\boldsymbol{Q_x = Q \times \frac{Sin(Tan^{-1}(Slope)}{Sin(Tan^{-1}(Slope)+Cos(Tan^{-1}(Slope)}}$$ and

$$\boldsymbol{Q_y = Q \times \frac{Cos(Tan^{-1}(Slope)}{Sin(Tan^{-1}(Slope)+Cos(Tan^{-1}(Slope)}} \quad \text{S4}$$

where Q_x *and* Q_y are the lateral fluxes in x- and y- directions, respectively, and *Slope* is the slope of the pixel obtained from the DEM.

The gravitational and matric potential induced water flow/seepage flux is one-dimensional according to Eq. S3, which is common in many distributed slope stability models (Alvioli and Baum, 2016; Alvioli et al., 2014; Alvioli et al., 2018; Van Asch et al., 1999; van Asch et al., 2009). Hydrological parameters, such as the saturated hydraulic conductivity, are given in a time history format. Once the spatial extent and other variables are provided to the numerical model, the precipitation boundary condition is imposed as a function of time. The total duration of the numerical simulation is decided by the duration of the precipitation\climate boundary conditions.

The solid materials of a debris flow begin to deposit when V is smaller than a critical flow velocity (V_e, m/s), and at the same time C_v is larger than $C_{v\infty}$.We use the V_e proposed by Takahashi et al. (1992):

$$\boldsymbol{V_e = \frac{2}{5d_L}\left(\frac{gsin\theta_e\rho}{0.02\rho_s}\right)^{0.5}\lambda^{-1}h^{1.5}} \quad \text{S5}$$

where g (m/s^2) is the gravity acceleration, h (m) is the flow height, θ_e (º) is the flattest slope on which a debris flow that comes down through the change in slope does not stop, and ρ (kg/m^3) is the bulk density of the debris flow. θ_e and ρ are defined as:

$$\boldsymbol{\theta_e = atan\left(\frac{C_v(\rho_s-\rho_w)tan\phi_{bed}}{C_v(\rho_s-\rho_w)+\rho_w}\right)} \quad \text{S6}$$

$$\boldsymbol{\rho = C_v(\rho_s - \rho_w) + \rho_w} \tag{S7}$$

Moreover:

$$\boldsymbol{\lambda^{-1} = \left(\frac{C_{v*}}{C_v}\right)^{1/3} - 1} \tag{S8}$$

The deposition rate (*i*, m/s) can be expressed as (Takahashi et al., 1992):

$$\boldsymbol{i = \delta_d \left(1 - \frac{V}{pV_e}\right) \frac{C_{V\infty} - C_V}{C_{V*}} V} \tag{S9}$$

where δ_d is a non-dimensional coefficient of deposition rate obtained through back-analysis and p(<1) is a non-dimensional coefficient to describe the initiation of the depositing process. A value of 0.67 for the latter is recommended by Takahashi et al. (1992).

Assuming turbulent flow conditions, which seem likely in steep and rough channels (Montogomery and Buffington, 1997), V is calculated using the Manning's equation when C_v is below an arbitrarily chosen limit of 0.4 (van Asch et al., 2014).

$$\boldsymbol{V = \frac{h^{2/3} sin\theta^{1/2}}{n}} \tag{S10}$$

where n ($m^{1/3}/s$) is the Manning's number equal to 0.04 (van Asch et al., 2014). For C_v > 0.4 (van Asch et al., 2014), a simple equation of motion is used:

$$\boldsymbol{\frac{\partial V}{\partial t} = g\left(sin\theta\, cos\theta - ktan\theta - S_f\right)} \tag{S11}$$

where k is the lateral pressure coefficient (taken equal to 1; van Asch et al. (2014), and S_f is a resistant factor depending on the rheology of the flow:

$$\boldsymbol{S_f = cos^2\theta\, tan\varphi' + \frac{1}{\rho g h}\left(\frac{3}{2}\tau_c + \frac{3\mu}{h} V\right)} \tag{S12}$$

where φ' (º) is the apparent friction angle of the flow for a certain pore water pressure, and μ (kPa·s) is its dynamic viscosity.

The spatially explicit rainfall timeseries maps from the WRF numerical model is shown in Fig.S1.

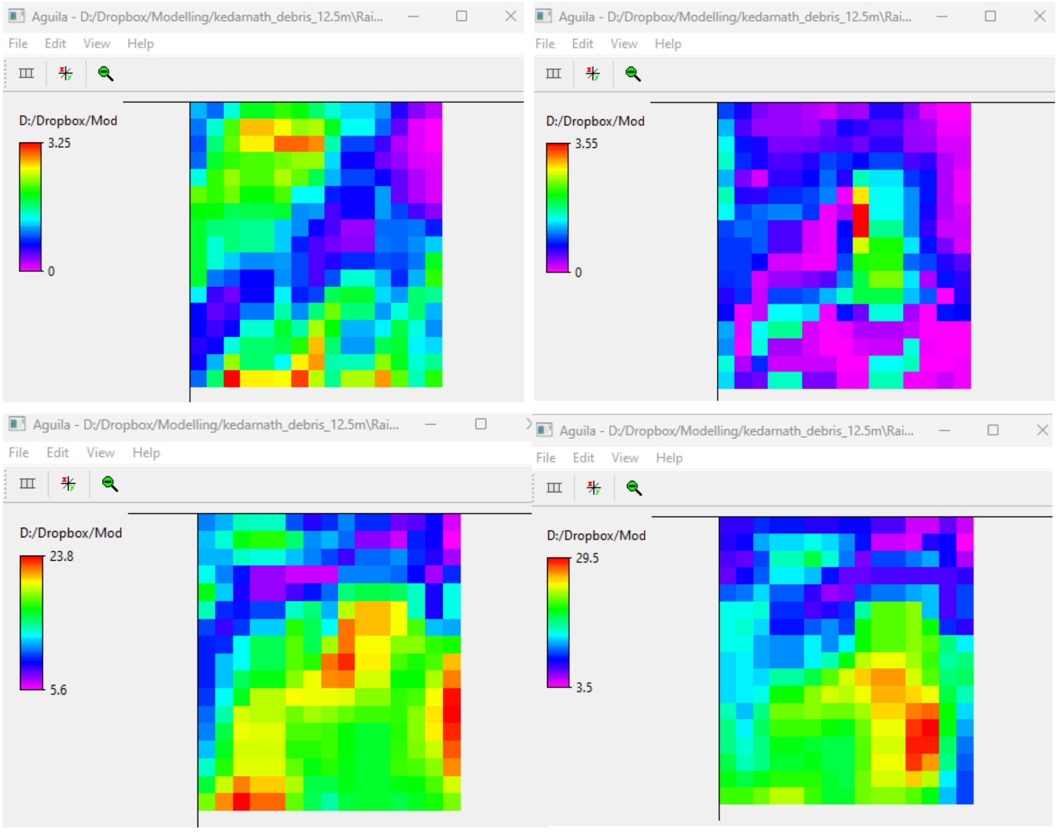

Figure S1 Spatially explicit timeseries of rainfall from WRF model at selected time intervals like 0-hour, 15 hour, 45 hours, and 62 hours. The total duration of the simulation is 72 hours. The grid spacing is at 1.8 km * 1.8 km. Rainfall units are in mm. Images plotted using the open source PCRaster Aguila visualisation tool (Pebesma et al., 2007): https://pcraster.geo.uu.nl/

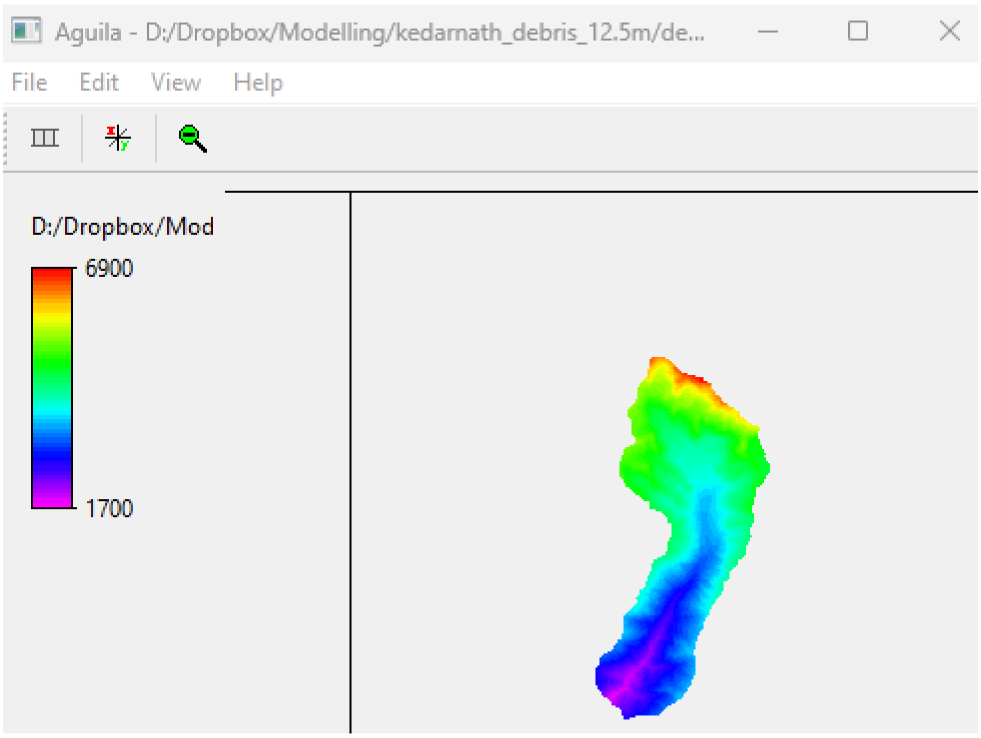

Figure S2 12.5m resolution digital elevation model keyed into the debris flow numerical model. The units are in m. a.s.l. Images plotted using the open source PCRaster Aguila visualisation tool (Pebesma et al., 2007): https://pcraster.geo.uu.nl/

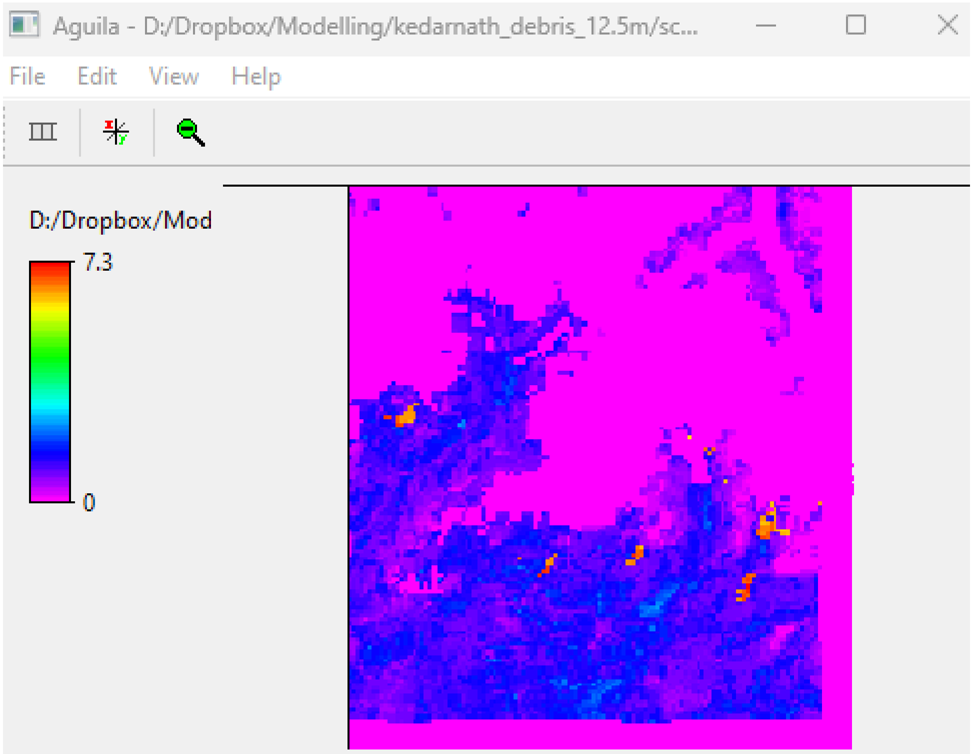

Figure S3 Input data of regolith/debris thickness into the debris flow numerical model. The units are in meters. Images plotted using the open source PCRaster Aguila visualisation tool (Pebesma et al., 2007): https://pcraster.geo.uu.nl/

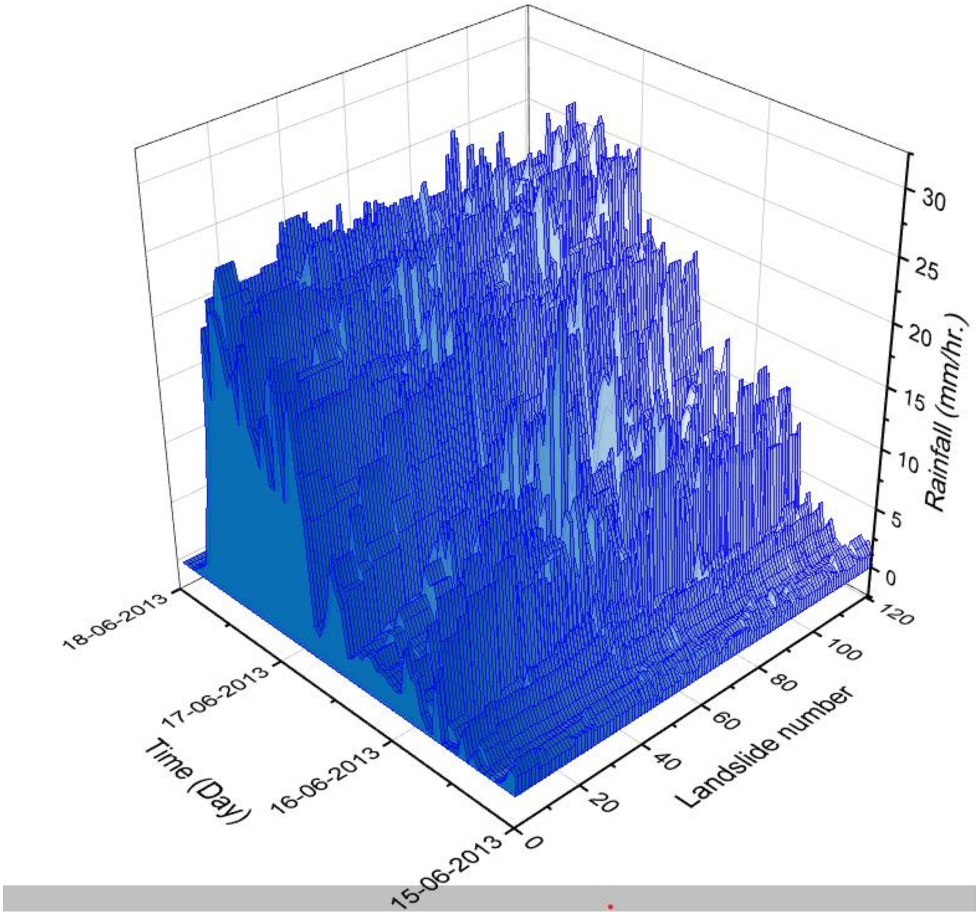

Figure S4 WRF modelled rainfall timeseries from 15 June 2013 to 17 June 2013 over the 121 landslides occurred in Kedarnath during the 2013 North India Floods. Plotted using Python in Jupyter Notebook (Kluyver et al., 2016)

IMD \ Coordinate	30.625_78.875	30.625_79.125	30.875_78.875	30.875_79.125
Count (Days)	10	10	10	10
Mean Rainfall	31.26391	33.209	30.15367	30.93523
std	27.1077	31.705075	26.597143	29.883263
Minimum Rainfall	5.8981	1.8681	7.9214	4.4819
25% Rainfall	13.3095	9.1688	11.73675	9.326925
50% Rainfall	19.6015	24.5115	19.2945	18.1685
75% Rainfall	50.4355	49.89675	44.98175	43.19875
Maximum Rainfall	84.3	89.709	89.087	90.521

WRF \ Coordinate	30.625_78.875	30.625_79.125	30.875_78.875	30.875_79.125
Count (Days)	10	10	10	10
Mean Rainfall	65.40172	62.229645	58.998149	50.734721
std	106.766135	105.084322	98.436804	85.882673
Minimum Rainfall	0.055902	0.022871	0.012269	0.00945
25% Rainfall	1.972491	1.901044	1.172568	0.849406
50% Rainfall	11.675601	8.307506	3.815687	3.056732
75% Rainfall	69.227324	63.235893	71.198019	58.808022
Maximum Rainfall	271.479065	291.634442	241.210433	221.94275

Figure S5 Comparison matrix of IMD data with WRF model output at daily timescales

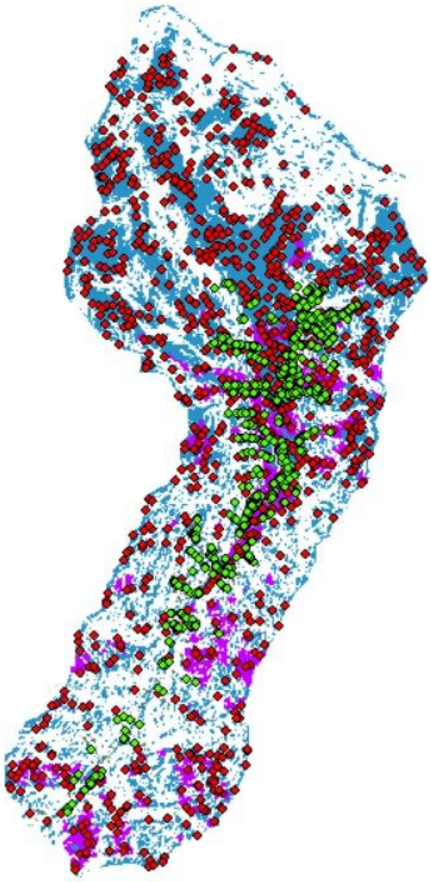

Figure S6 Random points used for accuracy assessment of the debris flow model. Image plotted using the open source PCRaster Aguila visualisation tool (Pebesma et al., 2007): https://pcraster.geo.uu.nl/

```
=== Detailed Accuracy By Class ===

                 TP Rate   FP Rate
                 0.484     0.226
                 0.774     0.516
Weighted Avg.    0.633     0.375

=== Confusion Matrix ===

   a   b   <-- classified as
 447 477 |   a = Yes
 221 755 |   b = No
```

Figure S7 Details of accuracy assessment with True Skill Statistics (TSS) Evaluation. Image plotted using open-source Waikato Environment for Knowledge Analysis (WEKA) (Eibe et al., 2016) https://www.cs.waikato.ac.nz/ml/weka/

```
weka.classifiers.trees.RandomTree -K 0 -M 1.0 -V 0.001 -S 1 -do-not-check-capabilities

Time taken to build model: 0.16 seconds

=== Evaluation on training set ===

Time taken to test model on training data: 0.09 seconds

=== Summary ===

Correctly Classified Instances        1202               63.2632 %
Incorrectly Classified Instances       698               36.7368 %
Kappa statistic                          0.2592
Mean absolute error                      0.4633
Root mean squared error                  0.4813
Relative absolute error                 92.7201 %
Root relative squared error             96.3047 %
Total Number of Instances             1900

=== Detailed Accuracy By Class ===

                 TP Rate  FP Rate  Precision  Recall   F-Measure  MCC      ROC Area  PRC Area  Class
                 0.484    0.226    0.669      0.484    0.562      0.269    0.629     0.575     Yes
                 0.774    0.516    0.613      0.774    0.684      0.269    0.629     0.590     No
Weighted Avg.    0.633    0.375    0.640      0.633    0.624      0.269    0.629     0.583

=== Confusion Matrix ===

   a   b   <-- classified as
 447 477 |   a = Yes
 221 755 |   b = No
```

Figure S8 Details of accuracy assessment using Kappa statistics. Image plotted using open-source Waikato Environment for Knowledge Analysis (WEKA) (Eibe et al., 2016) https://www.cs.waikato.ac.nz/ml/weka/

Intensity of Rainfall	
No rain	Rainfall amount realised in a day is 0.0 mm
Trace	Rainfall amount realised in a day is between 0.01 to 0.04 mm
Very light rain	Rainfall amount realised in a day is between 0.1 to 2.4 mm
Light rain	Rainfall amount realised in a day is between 2.5 to 7.5 mm
Moderate Rain	Rainfall amount realised in a day is between 7.6 to 35.5 mm
Rather Heavy	Rainfall amount realised in a day is between 35.6 to 64.4 mm
Heavy rain	Rainfall amount realised in a day is between 64.5 to 124.4 mm
Very Heavy rain	Rainfall amount realised in a day is between 124.5 to 244.4 mm
Extremely Heavy rain	Rainfall amount realised in a day is more than or equal to 244.5 mm
Exceptionally Heavy Rainfall	This term is used when the amount realised in a day is a value near about the highest recorded rainfall at or near the station for the month or season. However, this term will be used only when the actual rainfall amount exceeds 12 cm.
Rainy Day	Rainfall amount realised in a day is 2.5 mm or more.

Figure S9 Intensity classification of rainfall as per IMD glossary.

RAINFALL INTENSITY / वर्षा की तीव्रता		RAINFALL DISTRIBUTION / वर्षा का वितरण		PROBABILITY OF OCCURRENCE / घटित होने की संभावना		SPELL OF RAINFALL / वर्षा का दौर	
VERY LIGHT RAIN / बहुत हल्की वर्षा	TRACE - 2.4 mm	ISOLATED PLACES / कहीं-कहीं	ISOLATED (UPTO 25% AREA)	UNLIKELY	Up to 25%	INTENSE SPELL / तीव्र दौर	20-30 mm/hour
LIGHT RAIN / हल्की वर्षा	2.5- 15.5 mm	FEW PLACES / कुछ जगह	SCATTERED (BETWEEN 25-50% AREA)	LIKELY	26 to 50%		
MODERATE RAIN / मध्यम वर्षा	15.6 – 64.4 mm	MANY PLACES / अनेक जगह	FAIRLY WIDE SPREAD (BETWEEN 50-75% AREA)	VERY LIKELY	51 to 75%	VERY INTENSE SPELL / अति तीव्र दौर	30-50 mm/hour
HEAVY RAIN / भारी वर्षा	64.5- 115.5 mm						
VERY HEAVY RAIN / बहुत भारी वर्षा	115.6- 204.4 mm	MOST PLACES / अधिकांश जगह	WIDE SPREAD (MORE THAN 75% AREA)	MOST LIKELY	Above 75%	EXTREMELY INTENSE SPELL / अत्यंत तीव्र दौर	50-100 mm/hour
EXTREMELY HEAVY RAIN / अत्यंत भारी वर्षा	> 204.4 mm						

❖Heavy snow: 64.5 – 115.5 cm (in depth) & Very heavy snow: 115.6 – 204.4 cm (in depth). (As per the new guidelines w.e.f January 1, 2016).
❖Forecast and Warning for a particular day is valid from 0830 hours IST of day till 0830 hours IST of next day.

Figure S10 Intensity classification of spell of rainfall as per IMD glossary

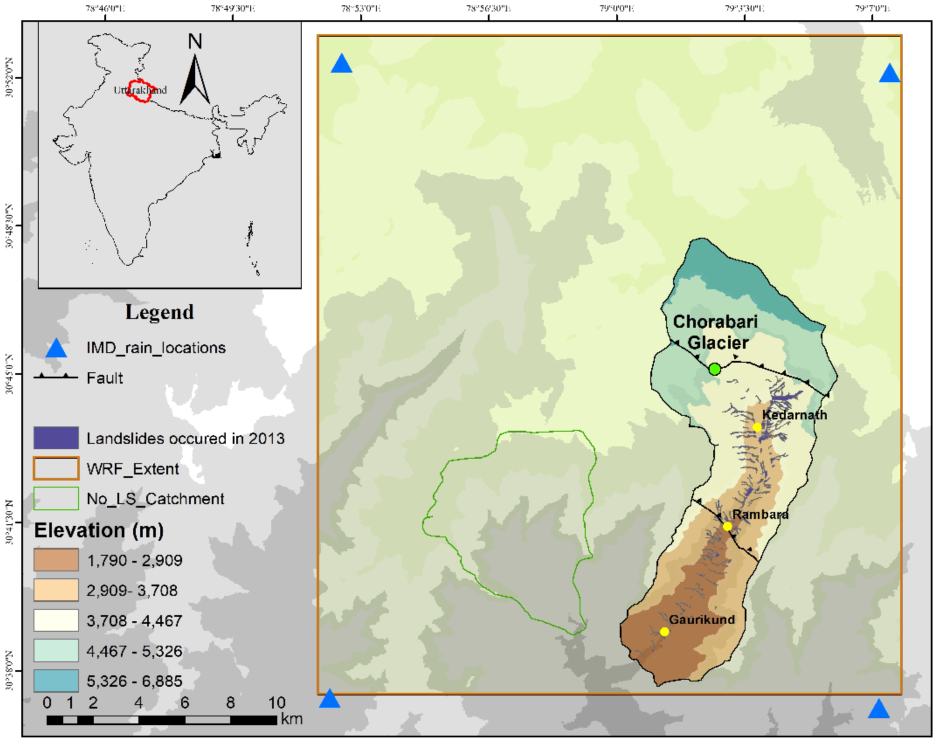

Figure S11 Map showing the small catchment area with no landslides within the analysis domain of WRF model. India administrative boundary highlighting Uttarakhand (Copyright: Survey of India, downloaded from: https://onlinemaps.surveyofindia.gov.in/Home.aspx, the Location of Uttarakhand (Copyright: Survey of India, downloaded from: https://onlinemaps.surveyofindia.gov.in/Home.aspx. Image plotted using ArcMap ArcGIS version 10.8.2.

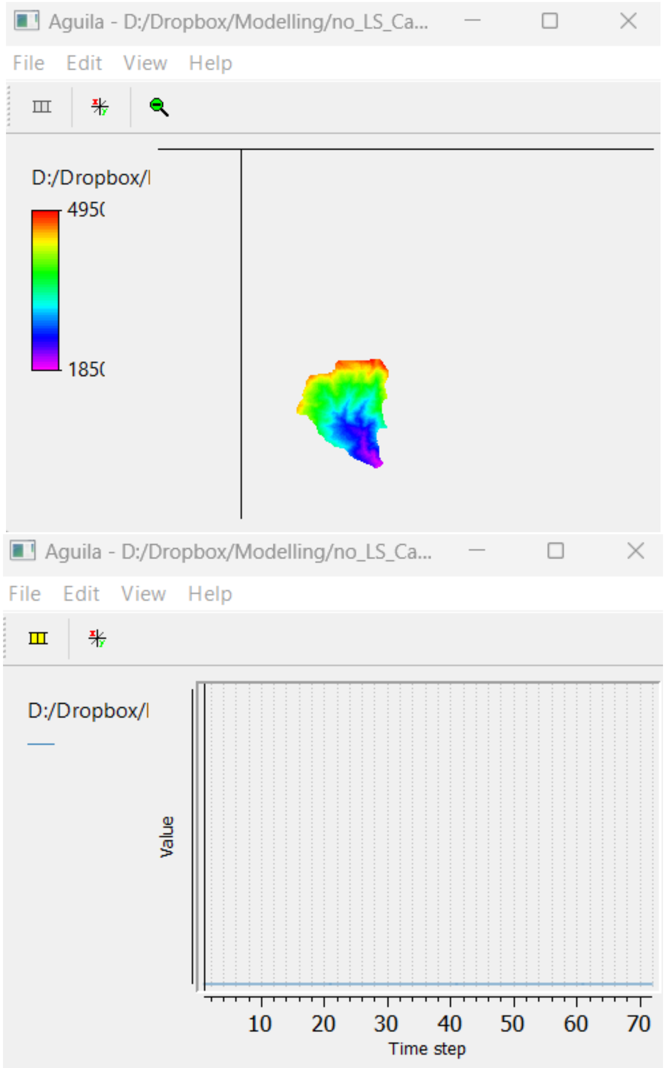

Figure S12 DEM and Debris flow volume =0 for the small catchment with no/less landslides. Images plotted using the open source PCRaster Aguila visualisation tool (Pebesma et al., 2007): https://pcraster.geo.uu.nl/

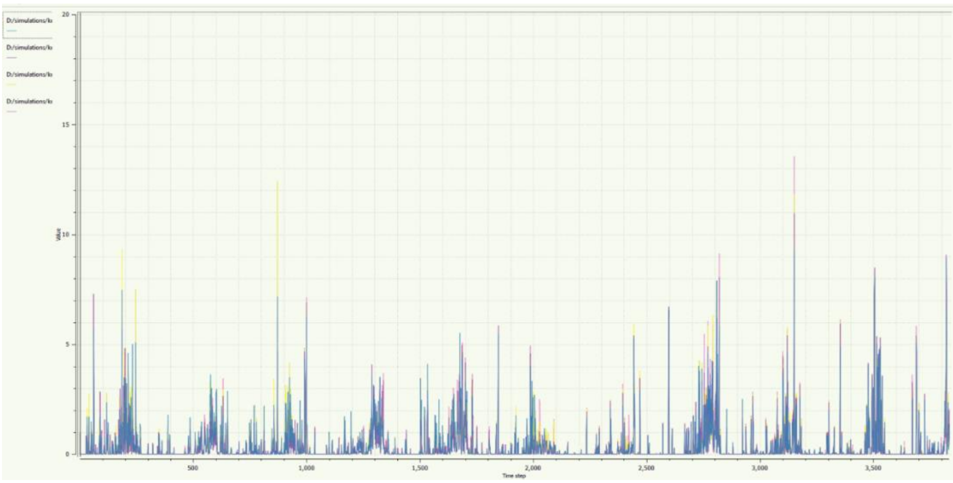

Figure S13 Daily rainfall data used for simulating moisture content at each pixel within the study area. Data is from 2003 to 2015. Image plotted using the open source PCRaster Aguila visualisation tool (Pebesma et al., 2007): https://pcraster.geo.uu.nl/

References

Alvioli, M. and Baum, R.L., 2016. Parallelization of the TRIGRS model for rainfall-induced landslides using the message passing interface. Environmental Modelling & Software, 81: 122-135.

Alvioli, M., Guzzetti, F. and Rossi, M., 2014. Scaling properties of rainfall induced landslides predicted by a physically based model. Geomorphology, 213: 38-47.

Alvioli, M., Melillo, M., Guzzetti, F., Rossi, M., Palazzi, E., von Hardenberg, J., Brunetti, M.T. and Peruccacci, S., 2018. Implications of climate change on landslide hazard in Central Italy. Sci Total Environ, 630: 1528-1543.

Beguería, S., Van Asch, T.W.J., Malet, J.P. and Gröndahl, S., 2009. A GIS-based numerical model for simulating the kinematics of mud and debris flows over complex terrain. Natural Hazards and Earth System Sciences, 9(6): 1897-1909.

Farrell, D.A. and Larson, W.E., 1972. Modeling the pore structure of porous media. Water Resources Research, 8(3): 699-706.

Quenta, G., Galaza, I., Teran, N., Hermanns, R.L., Cazas, A. and García, H., 2007. Deslizamiento traslacional y represamiento en el valle de Allpacoma, ciudad de La Paz, Bolivia. Movimientos en Masa en la Región Andina–Una Guía para la Evaluación de Amenazas, Proyecto Multinacional Andino: Geociencias para las Comunidades Andinas, Servicio Nacional de Geología y Minería, Santiago, Chile, Publicación Geológica Multinacional(4): 230-234.

Van Asch, T.W.J., Buma, J. and Van Beek, L.P.H., 1999. A view on some hydrological triggering systems in landslides. Geomorphology, 30(1): 25-32.

van Asch, T.W.J., Van Beek, L.P.H. and Bogaard, T.A., 2009. The diversity in hydrological triggering systems of landslides, pp. 8-10.

Alvioli M and Baum RL (2016) Parallelization of the trigrs model for rainfall-induced landslides using the message passing interface. Environmental Modelling & Software 81: 122-135. doi: https://doi.org/10.1016/j.envsoft.2016.04.002

Alvioli M, Guzzetti F and Rossi M (2014) Scaling properties of rainfall induced landslides predicted by a physically based model. Geomorphology 213: 38-47. doi: 10.1016/j.geomorph.2013.12.039

Alvioli M, Melillo M, Guzzetti F, Rossi M, Palazzi E, von Hardenberg J, Brunetti MT and Peruccacci S (2018) Implications of climate change on landslide hazard in central Italy. The Science of the total environment 630: 1528-1543. doi: 10.1016/j.scitotenv.2018.02.315

Beguería S, Van Asch TWJ, Malet JP and Gröndahl S (2009) A GIS-based numerical model for simulating the kinematics of mud and debris flows over complex terrain. Nat Hazards Earth Syst Sci 9: 1897-1909.

Bout, B., Lombardo, L., van Westen, C. J. & Jetten, V. G. (2018), 'Integration of two-phase solid fluid equations in a catchment model for flashfloods, debris flows and shallow slope failures', Environmental Modelling & Software 105, 1–16.

Brunner, G. W. (1995), Hec-ras river analysis system. hydraulic reference manual. version 1.0., Technical report, Hydrologic Engineering Center Davis CA.

Clement, M. A., Kilsby, C. & Moore, P. (2018), 'Multi-temporal synthetic aperture radar flood mapping using change detection', Journal of Flood Risk Management 11(2), 152–168.

Dhungel, S., Barber, M. E. & Mahler, R. L. (2019), 'Comparison of one-and two-dimensional flood modeling in urban environments', International journal of sustainable development and planning 14(4), 356–366.

Dom`enech, G., Fan, X., Scaringi, G., van Asch, T. W., Xu, Q., Huang, R. & Hales, T. C. (2019), 'Modelling the role of material depletion, grain coarsening and revegetation in debris flow occurrences after the 2008 Wenchuan earthquake', Engineering Geology 250, 34–44.

Eibe Frank, Mark A. Hall, and Ian H. Witten (2016). The WEKA Workbench. Online Appendix for "Data Mining: Practical Machine Learning Tools and Techniques", Morgan Kaufmann, Fourth Edition, 2016.

Farrell DA and Larson WE (1972) Modeling the pore structure of porous media. Water Resources Research 8: 699-706. doi: 10.1029/WR008i003p00699

Goutte, C. & Gaussier, E. (2005), A probabilistic interpretation of precision, recall and f-score, with implication for evaluation, in 'European conference on information retrieval', Springer, pp. 345–359.

Gorelick, N., Hancher, M., Dixon, M., Ilyushchenko, S., Thau, D. & Moore, R. (2017), 'Google earth engine: Planetary-scale geospatial analysis for everyone', Remote sensing of Environment 202, 18–27.

Karssenberg, D., Burrough, P. A., Sluiter, R. & de Jong, K. (2001), 'The PCRaster Software and Course Materials for Teaching Numerical Modelling in the Environmental Sciences', Transactions in GIS 5(2), 99–110. URL: https://onlinelibrary.wiley.com/doi/10.1111/1467-9671.00070

Kluyver, T., Ragan-Kelley, B., Fernando P'erez, Granger, B., Bussonnier, M., Frederic, J., … Willing, C. (2016). Jupyter Notebooks – a publishing format for reproducible computational workflows. In F. Loizides & B. Schmidt (Eds.), Positioning and Power in Academic Publishing: Players, Agents and Agendas (pp. 87–90).

Kuriakose SL, van Beek LPH and van Westen CJ (2009) Parameterizing a physically based shallow landslide model in a data-poor region. Earth Surf Process Landforms 34: 867-881. doi: 10.1002/esp.1794

Landis, J. R. & Koch, G. G. (1977), 'The measurement of observer agreement for categorical data', biometrics pp. 159–174.

Pebesma, E. J., de Jong, K., and Briggs, D.: Interactive visualization of uncertain spatial and spatio-temporal data under different scenarios: An air quality example, International Journal of Geographical Information Science 21(5), 515-527, 2007. doi: 10.1080/13658810601064009.

Quenta G, Galaza I, Teran N, Hermanns RL, Cazas A and García H (2007) Deslizamiento traslacional y represamiento en el valle de Allpacoma, ciudad de La Paz, Bolivia. Movimientos en Masa en la Región Andina–Una Guía para la Evaluación de Amenazas, Proyecto Multinacional Andino: Geociencias para las Comunidades Andinas, Servicio Nacional de Geología y Minería, Santiago, Chile, Publicación Geológica Multinacional: 230-234.

Siva Subramanian, S., Fan, X., Yunus, A., Van Asch, T., Scaringi, G., Xu, Q., Dai, L., Ishikawa, T. & Huang, R. (2020), 'A sequentially coupled catchment-scale numerical model for snowmelt-induced soil slope instabilities', Journal of Geophysical Research: Earth Surface 125(5), e2019JF005468.

Story, M. & Congalton, R. G. (1986), 'Accuracy assessment: a user's perspective', Photogrammetric Engineering and remote sensing 52(3), 397–399.

Sulal, Vishnu and Kumar T (2020) Note on the preliminary assessment of landslide at Pettimudi near Munnar, Idukki district, Kerala. GEOLOGICAL SURVEY OF INDIA, Thiruvananthapuram.

Takahashi, T. (2007), Debris flow: mechanics, prediction and countermeasures, Taylor & Francis.

Takahashi, T., Nakagawa, H., Harada, T. & Yamashiki, Y. (1992), 'Routing debris flows with particle segregation', Journal of Hydraulic Engineering 118(11), 1490–150